

Fermionic Dark Matter and New Scalar Production in $e^+e^- \rightarrow H^+H^-$ at Colliders

Asmaa AlMella^{1,*}, Faeq Abed^{2,*}, Gaber Faisel¹

¹ Department of Physics, Faculty of Arts and Sciences, Suleyman Demirel University, 32260, Isparta, Turkey.

Corresponding Author: Email: asmaa.almella@gmail.com - ORCID: 0000-0003-3975-3504,

Email: gaber.faisel@sdu.edu.tr - ORCID: 0000-0001-8770-1966.

²Iraqi Nuclear Regulatory Authority, Baghdad, Iraq.

Corresponding Author: Email: faeq.abed@irsra.gov.iq - ORCID: 0000-0002-3934-4367

Abstract

We investigate the pair production process $e^+e^- \rightarrow H^+H^-$ in the framework of the scotogenic model. The production mechanism receives contributions at tree level from photon and Z-boson exchange, as well as from t -channel exchange of the new singlet right-handed fermions $N_{1,2,3}$, where neutrino masses are generated radiatively and one of the singlet right-handed fermions serves as a viable dark matter candidate. We evaluate the individual contributions of these diagrams and compute the total production cross section after imposing all relevant theoretical and experimental constraints on the model parameters, including those associated with dark matter relic abundance and direct detection limits. Our results demonstrate that the dominant contribution to the cross section originates from the exchange of the singlet fermions $N_{1,2,3}$, particularly from the dark matter component of the spectrum. In addition, we examine the dependence of the cross section on the center-of-mass energy for several benchmark scenarios in the allowed parameter space. These predictions can be probed at future high-energy e^+e^- colliders, providing a sensitive test of the scotogenic framework and the role of fermionic dark matter, as well as enabling more stringent constraints on the model parameters.

Keywords: Scotogenic model, Dark matter, Neutrino masses, L^AT_EX, sample

DOI: XXXXXXXXXX

1. INTRODUCTION

The requirement for the existence of New Physics (NP) beyond the Standard Model (SM) arises from several fundamental limitations of the SM. Notably, the SM lacks a mechanism for generating neutrino masses and fails to provide a viable candidate for Dark Matter (DM). Additional shortcomings include the absence of gravity within the SM framework and its inability to account for the baryon asymmetry observed in the Universe. These deficiencies collectively highlight the need for extensions to the SM.

One of the prominent extensions of the Standard Model (SM) is the scotogenic model, introduced by Ma in 2006 [1]. This model offers a compelling mechanism for generating small neutrino masses, which is consistent with experimental observations. In addition to addressing the neutrino mass problem, the scotogenic model provides a viable candidate for dark matter (DM). Specifically, the DM candidate can originate from the new particles introduced by the model, including components of the scalar doublet η or the lightest of the three singlet Majorana fermions $N_{1,2,3}$. These additional particles, η and N_i , are proposed extensions to the particle content of the SM. A crucial feature of the model is the imposition of a Z_2 symmetry, under which all SM particles are Z_2 -even, while the newly introduced particles are Z_2 -odd. This symmetry ensures the stability of the DM candidate, further enhancing the model's consistency and appeal.

In Ref. [2], the process $e^+e^- \rightarrow H^+H^- \rightarrow \ell^+\ell^-\eta$ was investigated for potential collider signatures. With advancements over the past decade in neutrino oscillation experiments and

updated constraints on neutrino masses derived from cosmological observations, it is now possible to revise and refine the constraints presented in that study. Additionally, recent measurements of the dark matter relic density provide an essential new dataset to incorporate into the analysis, offering the potential for stronger constraints on the model.

Updating these constraints is crucial for accurately predicting the cross section of the process $e^+e^- \rightarrow H^+H^-$, which was not analyzed in Ref. [2]. This process is significant as the produced H^+H^- pair can decay into various final states with different particle combinations, all of which depend on the magnitude of the $e^+e^- \rightarrow H^+H^-$ cross section. Therefore, a thorough analysis of this cross section is essential.

In this study, we perform such an analysis, focusing on the individual contributions to the cross section from Z-boson exchange, photon exchange, and the new singlet fermions introduced by the scotogenic model. This comprehensive approach provides a more complete understanding of the process and its implications within the model.

2. THE SCOTOGENIC MODEL

The scotogenic model extends the Standard Model (SM) scalar sector by introducing an additional scalar doublet, η . The scalar sector of the scotogenic model is described by the following Lagrangian:

$$\mathcal{L} = (\mathcal{D}^\mu \Phi)^\dagger \mathcal{D}_\mu \Phi + (\mathcal{D}^\mu \eta)^\dagger \mathcal{D}_\mu \eta - \mathcal{V}, \quad (1)$$

where Φ represents the SM Higgs doublet, \mathcal{D}_μ is the covariant derivative that includes SM gauge fields, and \mathcal{V} denotes the scalar potential, given by [1]:

$$\begin{aligned} \mathcal{V} = & \mu_1^2 \Phi^\dagger \Phi + \mu_2^2 \eta^\dagger \eta + \frac{1}{2} \lambda_1 (\Phi^\dagger \Phi)^2 + \frac{1}{2} \lambda_2 (\eta^\dagger \eta)^2 \\ & + \lambda_3 (\Phi^\dagger \Phi)(\eta^\dagger \eta) + \lambda_4 (\Phi^\dagger \eta)(\eta^\dagger \Phi) + \frac{1}{2} \lambda_5 [(\Phi^\dagger \eta)^2 + (\eta^\dagger \Phi)^2], \end{aligned}$$

After electroweak symmetry breaking, the fields are expressed as:

$$\Phi = \begin{pmatrix} 0 \\ \frac{1}{\sqrt{2}}(h+v) \end{pmatrix}, \quad \eta = \begin{pmatrix} H^+ \\ \frac{1}{\sqrt{2}}(\mathcal{S} + i\mathcal{P}) \end{pmatrix}, \quad (2)$$

where h is the physical Higgs boson, and v is the vacuum expectation value (VEV) of Φ . Due to the imposed Z_2 symmetry, the VEV of η is zero.

The scalar masses are given by:

$$m_S^2 = m_{\mathcal{P}}^2 + \lambda_5 v^2 = \mu_2^2 + \frac{1}{2}(\lambda_3 + \lambda_4 + \lambda_5)v^2, \\ m_{H^\pm}^2 = \mu_2^2 + \frac{1}{2}\lambda_3 v^2.$$

In the limit of $|\lambda_5| \ll |\lambda_3 + \lambda_4|$, it follows that $m_S^2 \simeq m_{\mathcal{P}}^2$ [3].

The interactions and masses of the new singlet Majorana fermions (N_k) are described by the Lagrangian:

$$\mathcal{L}_N = -\frac{1}{2}M_k \overline{N_k^c} P_R N_k + \mathcal{Y}_{rk} \left[\bar{\ell}_r H^- - \frac{1}{\sqrt{2}}\bar{\nu}_r (\mathcal{S} - i\mathcal{P}) \right] P_R N_k + \text{H.c.}, \quad (3)$$

where $\ell_{1,2,3} = e, \mu, \tau$, \mathcal{Y}_{rk} are the Yukawa couplings, M_k represents the masses of N_k , $P_R = \frac{1}{2}(1 + \gamma_5)$, and $k, r = 1, 2, 3$.

The interactions of H^\pm with the photon (A) and Z-boson are derived from the Lagrangian:

$$\mathcal{L}_H^\pm \supset ie (H^+ \partial^\rho H^- - H^- \partial^\rho H^+) A_\rho \\ + \frac{g}{2c_w} [i(1 - 2s_w^2)(H^+ \partial^\rho H^- - H^- \partial^\rho H^+)] Z_\rho \quad (4)$$

where $e = gs_w$, $c_w = \cos \theta_W$, and $s_w = \sin \theta_W$, with θ_W being the Weinberg angle.

This framework establishes the key scalar and fermionic properties and interactions in the scotogenic model.

2.1. Neutrino masses generation

The imposed Z_2 symmetry in the scotogenic model prevents neutrino masses at the tree level. However, at the one-loop level, neutrino masses are generated through the mediation of \mathcal{S} , \mathcal{P} , and N_k . The eigenvalues of the light neutrino masses m_i are determined by the loop-induced quantity [1]:

$$\Lambda_k = \frac{\lambda_5 v^2}{16\pi^2 M_k} \left[\frac{M_k^2}{m_0^2 - M_k^2} + \frac{2M_k^4 \ln(M_k/m_0)}{(m_0^2 - M_k^2)^2} \right], \quad (5)$$

where $m_0 = \frac{1}{2}(m_S + m_{\mathcal{P}}) \simeq m_S \simeq m_{\mathcal{P}}$. The neutrino mass matrix is expressed as:

$$\mathcal{M}_\nu = Y \text{diag}(\Lambda_1, \Lambda_2, \Lambda_3) Y^T, \quad (6)$$

and it can be diagonalized by:

$$\text{diag}(m_1, m_2, m_3) = \mathcal{U}^\dagger \mathcal{M}_\nu \mathcal{U}^*, \quad (7)$$

where the unitary matrix \mathcal{U} represents the Pontecorvo-Maki-Nakagawa-Sakata (PMNS) matrix. In our analysis, the PDG parametrization [4] is utilized, given by $\mathcal{U} =$

$\tilde{u} \text{ diag}(e^{i\alpha_1/2}, e^{i\alpha_2/2}, 1)$, with $\alpha_{1,2}$ being the Majorana CP -violation phases, and \tilde{u} defined in terms of $c_{mn} = \cos \theta_{mn} \geq 0$, $s_{mn} = \sin \theta_{mn} \geq 0$, and the Dirac phase δ . The matrix \tilde{u} is detailed in Eq. (10) of Ref. [5]. Analytical solutions for Eqs. (??) are given by [2]:

$$Y_{e1} = \frac{-c_{12} c_{13} Y_1}{c_{12} c_{23} s_{13} e^{i\delta} - s_{12} s_{23}}, \quad Y_{e2} = \frac{-s_{12} c_{13} Y_2}{s_{12} c_{23} s_{13} e^{i\delta} + c_{12} s_{23}}, \\ Y_{\mu 1} = \frac{(c_{12} s_{23} s_{13} e^{i\delta} + s_{12} c_{23}) Y_1}{c_{12} c_{23} s_{13} e^{i\delta} - s_{12} s_{23}}, \quad Y_{\mu 3} = \frac{s_{23} Y_3}{c_{23}}, \\ Y_{e3} = \frac{s_{13} Y_3}{c_{23} c_{13} e^{i\delta}}, \quad Y_{\mu 2} = \frac{(s_{12} s_{23} s_{13} e^{i\delta} - c_{12} c_{23}) Y_2}{s_{12} c_{23} s_{13} e^{i\delta} + c_{12} s_{23}}, \\ Y_{\tau k} = Y_k, \quad (8)$$

which correspond to the light neutrino mass eigenvalues [2]:

$$m_1 = \frac{\Lambda_1 Y_{e1}^2 e^{-i\alpha_1}}{c_{12}^2 c_{13}^2}, \quad m_2 = \frac{\Lambda_2 Y_{e2}^2 e^{-i\alpha_2}}{s_{12}^2 c_{13}^2}, \quad m_3 = \frac{\Lambda_3 Y_3^2}{c_{13}^2 c_{23}^2}. \quad (9)$$

The Majorana CP -violation phases are determined using the relations:

$$\alpha_1 = \arg(\Lambda_1 Y_{e1}^2), \quad \alpha_2 = \arg(\Lambda_2 Y_{e2}^2), \quad \arg(\Lambda_3 Y_3^2) = 0. \quad (10)$$

2.2. Dark Matter

The scotogenic model extends the Standard Model (SM) by introducing additional particles in the fermionic and scalar sectors, specifically $N_{1,2,3}$ and S, P, H^\pm , respectively. These new particles are odd under the Z_2 symmetry, ensuring that the lightest among them is stable and can serve as a candidate for dark matter (DM).

In this study, we focus on the commonly considered scenario where N_1 acts as the DM particle, with N_2 nearly degenerate in mass with N_1 . This configuration is advantageous because it simultaneously satisfies the constraints from the DM relic density and the branching ratio (BR) of the lepton flavor-violating process $\mu \rightarrow e\gamma$.

The relic density is represented in terms of the current DM density relative to its critical value, Ω , and the Hubble parameter, \hat{h} , as $\Omega \hat{h}^2$. Theoretical estimation of this quantity follows the expression [3, 6]:

$$\Omega \hat{h}^2 = \frac{1.07 \times 10^9 x_f \text{ GeV}^{-1}}{\sqrt{g_*} m_{\text{Pl}} [a_{\text{eff}} + 3(b_{\text{eff}} - a_{\text{eff}}/4)/x_f]}, \\ x_f = \ln \frac{0.191 (a_{\text{eff}} + 6b_{\text{eff}}/x_f) M_1 m_{\text{Pl}}}{\sqrt{g_* x_f}} \quad (11)$$

Here, g_* is the effective number of relativistic degrees of freedom below the freeze-out temperature $T_f = M_1/x_f$, and $m_{\text{Pl}} = 1.22 \times 10^{19} \text{ GeV}$ is the Planck mass. The parameters a_{eff} and b_{eff} are derived from the expansion of the coannihilation rate, $\sigma_{\text{eff}} v_{\text{rel}} = a_{\text{eff}} + b_{\text{eff}} v_{\text{rel}}^2$, in terms of the relative speed v_{rel} of the annihilating particles in their center-of-mass frame. The

effective cross-section is given as $\sigma_{eff} = \frac{1}{4}(\sigma_{11} + \sigma_{12} + \sigma_{21} + \sigma_{22})$, where the individual cross sections σ_{ij} (for $i, j = 1, 2$) are expressed as:

$$\sigma_{ij} = \sigma_{N_i N_j \rightarrow \ell_i^- \ell_j^+} + \sigma_{N_i N_j \rightarrow \nu_i \nu_j} \quad (12)$$

The above cross sections have been computed in Refs.[7, 2] and arise from t - and u -channel tree-level diagrams mediated by H^\pm and $(\mathcal{S}, \mathcal{P})$, depending on whether the final states are charged leptons or neutral neutrinos.

In our analysis, to constrain the parameter space of the model using the observed DM relic density, we assume that the DM and the new scalar particles are not degenerate in mass. This avoids the contributions of scalar co-annihilation processes to the relic density.

2.3. $e^+(p_+) e^-(p_-) \rightarrow H^+ H^-$

In the scotogenic model considered in this study, the amplitude for the process $e^+(p_+) e^-(p_-) \rightarrow H^+ H^-$, receives contributions from tree-level diagrams involving the exchange of a photon (γ), a Z boson, and $N_{1,2,3}$. Assuming massless e^\pm , the resulting cross section is expressed as [2].

$$\begin{aligned} \sigma_{e^+ e^- \rightarrow H^+ H^-} = & \frac{\pi \alpha^2 \beta^3}{3s} + \frac{\alpha}{12} \frac{(g_L^2 + g_L g_R) \beta^3}{s - m_Z^2} + \frac{(g_L^4 + g_L^2 g_R^2) \beta^3}{96\pi (s - m_Z^2)^2} \\ & + \sum_k \frac{|\mathcal{Y}_{1k}|^4}{64\pi s} \left(w_k \ln \frac{w_k + \beta}{w_k - \beta} - 2\beta \right) + \left[\frac{\alpha}{16s} + \frac{g_L^2}{64\pi (s - m_Z^2)} \right] \\ & \sum_k |\mathcal{Y}_{1k}|^2 \left[(w_k^2 - \beta^2) \ln \frac{w_k + \beta}{w_k - \beta} - 2\beta w_k \right] \\ & + \sum_{j,k > j} \frac{|\mathcal{Y}_{1j} \mathcal{Y}_{1k}|^2}{64\pi s} \left(\frac{w_j^2 - \beta^2}{w_j - w_k} \ln \frac{w_j + \beta}{w_j - \beta} + \frac{w_k^2 - \beta^2}{w_k - w_j} \ln \frac{w_k + \beta}{w_k - \beta} \right. \\ & \left. - 2\beta \right) \end{aligned} \quad (13)$$

here $j, k = 1, 2, 3$, $s = (p_+ + p_-)^2$, $\alpha = \frac{e^2}{4\pi}$, $\beta = \sqrt{1 - \frac{4m_H^2}{s}}$ and $w_k = 1 + \frac{2M_k^2}{s} - \frac{2m_H^2}{s} \beta$. In the numerical analysis, we employ the effective values $\alpha = 1/128$, $g = 0.6517$, and $s_w^2 = 0.23146$ [4].

2.4. Constraints

In this study, we adopt the normal ordering (NO) of neutrino masses. The mixing angles, Dirac phase, $|\Delta m_{31}^2|$, and Δm_{21}^2 are determined from various measurements. For numerical evaluation, we use the results of the global neutrino oscillation data fit presented in Ref. [8]. This fit imposes the constraint $32.0 < R_m \equiv \frac{|\Delta m_{31}^2|}{\Delta m_{21}^2} < 36.0$ on the parameter space, based on the 90% CL ranges of the data. Additionally, measurements from the Planck satellite, BAO observations, H(z) data, and Supernovae Ia impose a stringent 2σ upper limit of $\sum m_i < 0.12$ eV. Constraints from neutrinoless double beta decay experiments yield $|\langle m \rangle_{ee}| < 0.06 - 0.2$ eV at the (95 hundred percent) confidence level [9, 10, 11], where $\langle m \rangle_{ee}$ is defined as $\langle m \rangle_{ee} = m_1 U_{e1}^2 + m_2 U_{e2}^2 + m_3 U_{e3}^2$.

The Yukawa interactions, which include the charged Higgs H^\pm as shown in Eq.(3), generate one-loop diagrams contributing to lepton flavor violation (LFV) processes. Detailed discussions of these processes are provided in Ref. [12]. Currently, experimental upper bounds on the branching ratios of such processes are $BR(\mu \rightarrow e\gamma) < 4.2 \times 10^{-13}$ [13], $BR(\tau \rightarrow e\gamma) < 3.3 \times 10^{-8}$ [14], and $BR(\tau \rightarrow \mu\gamma) < 4.4 \times 10^{-8}$ [14], with the most stringent constraint arising from $BR(\mu \rightarrow e\gamma)$. The expressions for these branching ratios in the scotogenic model are available in Ref. [12]. Meanwhile, the flavor-diagonal counterparts of these LFV processes modify the anomalous magnetic moment a_ℓ , as [15]:

$$\Delta a_{\ell_i} = \frac{-m_{\ell_i}^2}{16\pi^2 m_H^2} \sum_k |\mathcal{Y}_{ik}|^2 \mathcal{F}(M_k^2/m_H^2). \quad (14)$$

It is observed that the anomalous magnetic moment of the muon provides a stronger bound on the scotogenic parameter space compared to those from the electron and tau. The difference between the SM prediction and the current experimental value for a_μ is $a_\mu^{\text{exp}} - a_\mu^{\text{SM}} = (2.51 \pm 0.59) \times 10^{-9}$ [16].

Direct detection of dark matter (DM) via the interaction of N_1 with nucleons, mediated by Higgs exchange at one-loop level, is discussed in Ref. [17]. To evade stringent constraints from direct detection [18, 19], we follow Ref. [17, 20] and set $\lambda_{3,4} = 0.01$. Consequently, $m_0 \simeq m_{H^\pm} + \frac{1}{2}\lambda_4 v^2 \simeq m_{H^\pm} + 350$ GeV. Notably, direct detection bounds were not accounted for in Refs. [2]. However, in this study, these bounds are included alongside the latest global neutrino oscillation data from Ref. [8].

In the following section, we will present our results and analyze the implications. First, the mixing angles $\theta_{12,23,13}$ and Dirac phase δ are fixed to their central values based on the global neutrino oscillation data in Ref. [8]. Subsequently, a scan is performed over the model's parameter space, including the masses of the new scalars m_H, m_0 , the singlet fermions $N_{1,2,3}$, and the input parameters $\mathcal{Y}_{1,2,3}$ appearing in the Yukawa couplings listed in Eq.(8). For light DM masses $M_1 < 100$ GeV, LFV processes [21] and LHC searches [22, 23] predominantly exclude the parameter space. Concerning scalar masses, data on W and Z widths and the absence of direct evidence for new particles at e^+e^- colliders impose the following upper bounds [24, 25, 26]:

$$m_{H^\pm} + m_{\mathcal{S}, \mathcal{P}} > m_{W^\pm}, m_{H^\pm} > 70 \text{ GeV}, m_{\mathcal{S}} + m_{\mathcal{P}} > m_Z. \quad (15)$$

One should remark that there are constraints on the charged Higgs mass from the $\beta \rightarrow \tau\nu, \beta \rightarrow s\gamma$ and from the direct measurements of the charged Higgs decays at the LHC. In our analysis, we take into account all these constraints.

3. RESULTS AND DISCUSSIONS

This study considers the normal ordering (NO) of neutrino masses. The mixing angles, Dirac phase, $|\Delta m_{31}^2|$, and Δm_{21}^2 are constrained by various measurements. For numerical evaluations, the global neutrino oscillation data fit from Ref. [8] is used. The fit imposes the condition $32.0 < R_m \equiv \frac{|\Delta m_{31}^2|}{\Delta m_{21}^2} < 36.0$ at the 90% CL. Furthermore, data from the Planck satellite, BAO observations, H(z) measurements, and Supernovae Ia restrict the sum of neutrino masses to $\sum m_i < 0.12$ eV at 2σ . Neutrinoless double beta decay experiments constrain

$|\langle m \rangle_{ee}|$ to the range $0.06 - 0.2$ eV (95% CL) [9, 10, 11], where $\langle m \rangle_{ee} = m_1 U_{e1}^2 + m_2 U_{e2}^2 + m_3 U_{e3}^2$.

The Yukawa interactions involving the charged Higgs H^\pm , as described in Eq.(3), generate one-loop diagrams contributing to lepton flavor violation (LFV) processes. These are discussed in Ref. [12]. Current experimental upper bounds on the branching ratios of such processes include $\text{BR}(\mu \rightarrow e\gamma) < 4.2 \times 10^{-13}$ [13], $\text{BR}(\tau \rightarrow e\gamma) < 3.3 \times 10^{-8}$ [14], and $\text{BR}(\tau \rightarrow \mu\gamma) < 4.4 \times 10^{-8}$ [14], with the most stringent constraint arising from $\text{BR}(\mu \rightarrow e\gamma)$. Branching ratio expressions in the scotogenic model are detailed in Ref. [12]. The flavor-diagonal counterparts of these LFV processes alter the anomalous magnetic moment a_{ℓ_i} as [15]:

$$\Delta a_{\ell_i} = \frac{-m_{\ell_i}^2}{16\pi^2 m_H^2} \sum_k |Y_{ik}|^2 \mathcal{F}(M_k^2/m_H^2). \quad (16)$$

The muon anomalous magnetic moment places stronger constraints on the scotogenic parameter space than the electron or tau. The difference between the experimental and SM values is $a_{\mu}^{\text{exp}} - a_{\mu}^{\text{SM}} = (2.51 \pm 0.59) \times 10^{-9}$ [16].

Direct dark matter (DM) detection, mediated by Higgs exchange at the one-loop level, is discussed in Ref. [17]. To avoid stringent detection constraints [18, 19], we adopt $\lambda_{3,4} = 0.01$, following Refs. [17, 20], leading to $m_0 \simeq m_{H^\pm} + \frac{1}{2}\lambda_4 v^2 \simeq m_{H^\pm} + 350$ GeV. While previous works, such as Ref. [2], did not consider direct detection bounds, they are included here along with the latest global neutrino oscillation data [8].

The results and implications are presented next. The mixing angles $\theta_{12,23,13}$ and Dirac phase δ are fixed to their central values from Ref. [8]. A scan over the parameter space includes scalar masses m_H, m_0 , singlet fermions $N_{1,2,3}$, and Yukawa parameters $Y_{1,2,3}$ from Eq.(8). For $M_1 < 100$ GeV, LFV processes [21] and LHC searches [22, 23] largely exclude the parameter space. Constraints on scalar masses from W and Z decays and e^+e^- collider data impose limits [24, 25, 26]:

$$m_{H^\pm} + m_{S,P} > m_{W^\pm}, m_{H^\pm} > 70 \text{ GeV}, m_S + m_P > m_Z. \quad (17)$$

Subsequent sections explore the allowed parameter regions under individual and combined constraints, presented visually in figures such as Figs. 1, 2, 3, and 4. Finally, the study investigates predictions for $\sigma_{e^+e^- \rightarrow H^+H^-}$ cross-sections, benchmarked against constraints, with detailed contributions from Z , photon, and new fermions $N_{1,2,3}$ (Figs. 5 and 6).

Our analysis begins by fixing the neutrino mixing angles $\theta_{12}, \theta_{23}, \theta_{13}$ and the Dirac CP phase δ to their central values obtained from the latest global fit to neutrino oscillation data [8]. We then perform a systematic scan over the relevant parameter space of the model, which includes the masses of the singlet fermions $N_{1,2,3}$, the scalar masses m_H and m_0 , and the Yukawa coupling parameters $Y_{1,2,3}$.

As discussed previously, direct collider searches impose lower bounds on the scalar masses. In particular, for light dark matter scenarios with $M_1 < 100$ GeV, where N_1 is identified as the dark matter candidate, the parameter space is strongly constrained by lepton flavor violation processes [21] as well as by direct searches at the LHC [22, 23]. These constraints exclude most of the viable region in this mass range. Consequently, we impose a conservative lower bound of 100 GeV on all scalar masses.

Regarding the singlet fermions, the dark matter candidate N_1 remains largely unconstrained by current collider searches. In contrast, the masses of the heavier fermions N_2 and N_3 are required to be sufficiently large in order to satisfy the stringent bounds from lepton flavor violating observables, as will be demonstrated in the following.

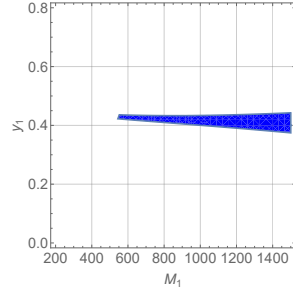


FIGURE 1: Region in magenta color is allowed by $\mu \rightarrow e\gamma$ constraint for the parameters $M_2 = M_1$, $M_3 = M_1 + 380$ GeV, $m_H = M_1 + 400$ GeV, $Y_2 = 0.49$ and $Y_3 = 0.66$.

In Fig. 1, the blue-shaded region is consistent with the $\mu \rightarrow e\gamma$ constraint, where the remaining parameters are fixed as $M_2 = M_1$, $M_3 = M_1 + 380$ GeV, $m_H = M_1 + 400$ GeV, $Y_2 = 0.49$ and $Y_3 = 0.66$. It is evident from the figure that satisfying the $\mu \rightarrow e\gamma$ bound requires a heavy charged Higgs mass as well as large masses for the fermions $N_{1,2,3}$.

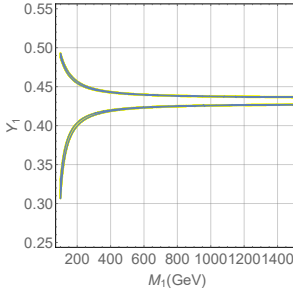


FIGURE 2: Allowed regions after imposing $\frac{|\Delta m_{31}^2|}{\Delta m_{21}^2}$ constraints for the choice of the parameters as $M_2 = M_1$, $M_3 = M_1 + 380$ GeV, $m_0 = M_1 + 750$ GeV, $Y_2 = 0.49$ and $Y_3 = 0.66$.

In Fig. 2, we present the allowed parameter regions after imposing the constraint on $\frac{|\Delta m_{31}^2|}{\Delta m_{21}^2}$. In this figure, the parameters are fixed to $M_2 = M_1$, $M_3 = M_1 + 380$ GeV, $m_0 = M_1 + 750$ GeV, $Y_2 = 0.49$ and $Y_3 = 0.66$. The shaded regions in the M_1 - Y_1 plane are consistent with the required constraint.

We now proceed to show the allowed region in the M_1 - Y_1 plane imposed by the dark matter relic density constraint Ωh^2 . The results are displayed in Fig. 3 for the parameter choice $M_2 = M_1$, $M_3 = M_1 + 380$ GeV, $m_H = M_1 + 400$ GeV, $m_0 = M_1 + 750$ GeV, $Y_2 = 0.49$ and $Y_3 = 0.66$. As illustrated in the figure, larger values of the dark matter mass M_1 require correspondingly larger values of the coupling Y_1 in order to satisfy the relic density bound. However, this requirement is not favored by the other constraints discussed above.

It is worth emphasizing that, in the previous figures presented above, we examined the impact of each individual constraint on the parameter space separately. Nevertheless, the viable parameter space must satisfy all relevant constraints simultaneously. Accordingly, in Fig. 4, we present the allowed

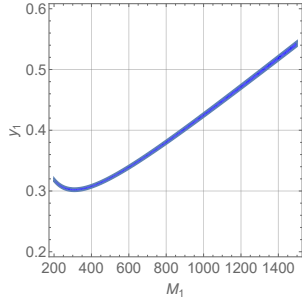


FIGURE 3: Allowed regions in the $M_1 - Y_1$ plane by $\Omega \hat{h}^2$ constraints for the parameters $M_2 = M_1$, $M_3 = M_1 + 380$ GeV, $m_H = M_1 + 400$ GeV, $m_0 = M_1 + 750$ GeV, $Y_2 = 0.49$ and $Y_3 = 0.66$.

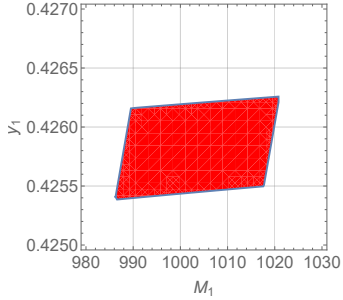


FIGURE 4: Allowed regions in the $M_1 - Y_1$ plane by $\mu \rightarrow e\gamma$, $\frac{|\Delta m_{31}^2|}{\Delta m_{21}^2}$, $\Omega \hat{h}^2$ constraints $M_2 = M_1$, $M_3 = M_1 + 380$ GeV, $m_H = M_1 + 400$ GeV, $m_0 = M_1 + 750$ GeV, $Y_2 = 0.49$ and $Y_3 = 0.66$.

region in the $M_1 - Y_1$ plane after imposing the dominant constraints arising from $\mu \rightarrow e\gamma$, $\frac{|\Delta m_{31}^2|}{\Delta m_{21}^2}$, and the dark matter relic density Ωh^2 . The red-colored region in the figure simultaneously satisfies all these constraints. From this region, we infer that viable solutions exist for which the masses of the new particles in the model are close to or above the 1 TeV scale. Furthermore, this region can be used to define a set of benchmark points that fulfill all imposed constraints on the model parameter space and thus allow predictions for the cross section $\sigma_{e^+e^- \rightarrow H^+H^-}$, which can be probed at future collider experiments. In Fig. 5, we show the individual contributions of the Z boson, photon, and the new singlet fermions $N_{1,2,3}$ to the cross section $\sigma_{e^+e^- \rightarrow H^+H^-}$ as functions of the center-of-mass energy \sqrt{s} , represented by the red, orange, and magenta curves, respectively. The results correspond to one of the allowed benchmark points in the parameter space, namely $M_1 = 1005$ GeV, $M_2 \simeq M_1 = 1005.0000035$ GeV, $M_3 = 1385$ GeV, $m_H = 1405$ GeV, $Y_1 = 0.4258$, $Y_2 = 0.49$, and $Y_3 = 0.66$. It is evident from the figure that the Z-boson contribution is the smallest, while the contributions mediated by the singlet fermions $N_{1,2,3}$ dominate the cross section. Finally, in Fig. 6, we present the total cross section $\sigma_{e^+e^- \rightarrow H^+H^-}$ as a function of the center-of-mass energy \sqrt{s} , shown in orange, blue, and red colors, respectively. As in the previous case, the figure corresponds to the same benchmark point in the parameter space. As can be observed, the cross section increases with increasing center-of-mass energy, reaches a maximum, and then decreases as \sqrt{s} continues to grow.

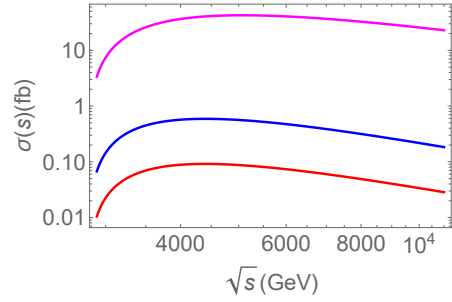


FIGURE 5: Z, photon and new singlet fermions $N_{1,2,3}$ individual contributions to the cross section of $\sigma_{e^+e^- \rightarrow H^+H^-}$ in red, orange and magenta colors respectively. The plots correspond to the allowed parameters $M_1 = 1005$ GeV, $M_2 \simeq M_1 = 1005.0000035$ GeV, $M_3 = 1385$ GeV, $m_H = 1405$ GeV, $Y_1 = 0.4258$, $Y_2 = 0.49$ and $Y_3 = 0.66$.

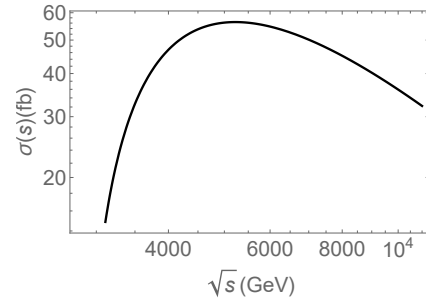


FIGURE 6: Total cross section $\sigma_{e^+e^- \rightarrow H^+H^-}$. The plots correspond to the allowed parameters $M_1 = 1005$ GeV, $M_2 \simeq M_1 = 1005.0000035$ GeV, $M_3 = 1385$ GeV, $m_H = 1405$ GeV, $Y_1 = 0.4258$, $Y_2 = 0.49$ and $Y_3 = 0.66$.

that satisfying $\frac{|\Delta m_{31}^2|}{\Delta m_{21}^2}$ constraints requires values of $Y_{1,2}$ roughly of order $\mathcal{O}(10^{-2})$ and Y_3 of order $\mathcal{O}(10^{-1})$. On the other hand, satisfying $\mu \rightarrow e\gamma$ constraints requires values of $Y_{1,2,3}$ roughly of order $\mathcal{O}(10^{-1})$. For satisfying $\Omega \hat{h}^2$ constraints, values of $Y_{2,3}$ roughly of order $\mathcal{O}(10^{-1})$ and Y_1 of order $\mathcal{O}(10^1)$ are required. It is known that $\mu \rightarrow e\gamma$ and $\Omega \hat{h}^2$ constraints can be simultaneously satisfied if the lightest singlet fermion is almost degenerated with the next to lightest singlet fermions. However, this possibility should be reexamined after taking into account the strong constraints from $\frac{|\Delta m_{31}^2|}{\Delta m_{21}^2}$. Finally, it is possible to have points satisfying all constraints for masses of new particles higher than 1 TeV. However, their impact on other processes will be small making them less relevant to explore new physics scenarios.

4. CONCLUSION

In this study, we explored the process $e^+e^- \rightarrow H^+H^-$ within the framework of the scotogenic model. The contributions to the amplitude of this process arise from tree-level diagrams mediated by the photon, the Z boson, and the right-handed fermions $N_{1,2,3}$. We analyzed the processes that can impose significant constraints on the parameter space relevant to $e^+e^- \rightarrow H^+H^-$. Additionally, we evaluated the individual contributions of the photon, the Z boson, and the right-handed fermions $N_{1,2,3}$ to the cross section of $e^+e^- \rightarrow H^+H^-$, incorporating

all stringent constraints on the model's parameters. Our results indicate that the dominant contribution to the cross section originates from the new singlet right-handed fermions $N_{1,2,3}$. Furthermore, we examined how the cross section varies with the center-of-mass energy for a set of benchmark points within the model's parameter space that adhere to the stringent bounds. Future e^+e^- colliders will investigate the process $e^+e^- \rightarrow H^+H^-$, offering opportunities to test our predictions by either imposing stricter constraints or confirming these results.

References

- [1] E. Ma, Phys. Rev. D **73**, 077301 (2006).
- [2] S. Y. Ho and J. Tandean, Phys. Rev. D **89**, 114025 (2014).
- [3] J. Kubo, E. Ma and D. Suematsu, Phys. Lett. B **642**, 18 (2006).
- [4] J. Beringer *et al.* [Particle Data Group Collaboration], Phys. Rev. D **86**, 010001 (2012).
- [5] G. Faisel, S. Y. Ho and J. Tandean, Phys. Lett. B **738**, 380-385 (2014).
- [6] G. Jungman, M. Kamionkowski, and K. Griest, Phys. Rept. **267**, 195 (1996).
- [7] S. Y. Ho and J. Tandean, Phys. Rev. D **87**, 095015 (2013).
- [8] P. F. de Salas, D. V. Forero, S. Gariazzo, P. Martínez-Miravé, O. Mena, C. A. Ternes, M. Tórtola and J. W. F. Valle, JHEP **02**, 071 (2021).
- [9] G. Anton *et al.* [EXO-200], Phys. Rev. Lett. **123**, no.16, 161802 (2019).
- [10] A. Gando *et al.* [KamLAND-Zen], Phys. Rev. Lett. **117**, no.8, 082503 (2016).
- [11] M. Agostini *et al.* [GERDA], Phys. Rev. Lett. **125**, no.25, 252502 (2020).
- [12] T. Toma and A. Vicente, JHEP **01**, 160 (2014).
- [13] A. M. Baldini *et al.* [MEG], Eur. Phys. J. C **76**, no.8, 434 (2016).
- [14] B. Aubert *et al.* [BaBar], Phys. Rev. Lett. **104**, 021802 (2010).
- [15] E. Ma and M. Raidal, Phys. Rev. Lett. **87**, 011802 (2001) [Erratum-*ibid.* **87**, 159901 (2001)].
- [16] T. Aoyama, N. Asmussen, M. Benayoun, J. Bijnens, T. Blum, M. Bruno, I. Caprini, C. M. Carloni Calame, M. Cè and G. Colangelo, *et al.* Phys. Rept. **887**, 1-166 (2020).
- [17] A. Ibarra, C. E. Yaguna and O. Zapata, Phys. Rev. D **93**, no.3, 035012 (2016).
- [18] E. Aprile *et al.* [XENON], Phys. Rev. Lett. **121**, no.11, 111302 (2018).
- [19] Y. Meng *et al.* [PandaX-4T], Phys. Rev. Lett. **127**, no.26, 261802 (2021).
- [20] J. Liu, Z. L. Han, Y. Jin and H. Li, JHEP **12**, 057 (2022) doi:10.1007/JHEP12(2022)057 [arXiv:2207.07382 [hep-ph]].
- [21] A. Vicente and C. E. Yaguna, JHEP **02**, 144 (2015).
- [22] G. Aad *et al.* [ATLAS], Phys. Rev. D **101**, no.5, 052005 (2020).
- [23] A. M. Sirunyan *et al.* [CMS], JHEP **04**, 123 (2021).
- [24] A. Arhrib, R. Benbrik, and N. Gaur, Phys. Rev. D **85**, 095021 (2012).
- [25] Q.H. Cao, E. Ma, and G. Rajasekaran, Phys. Rev. D **76**, 095011 (2007).
- [26] A. Pierce and J. Thaler, JHEP **0708**, 026 (2007) [hep-ph/0703056 [HEP-PH]]; E.M. Dolle and S. Su, Phys. Rev.

D **80**, 055012 (2009).